# Direct measurement of sea ice thermal conductivity: No surface reduction

D. J. Pringle,[1,2] H. J. Trodahl,[1] and T. G. Haskell[3]

Received 6 April 2005; revised 16 January 2006; accepted 6 February 2006; published 27 May 2006.

[1] We present new laboratory measurements of the thermal conductivity of small cores of landfast first-year (FY) and multiyear (MY) sea ice from McMurdo Sound, Antarctica. The conductivity of surface (0–10 cm) and subsurface (45–55 cm) FY ice, 2.14 ± 0.11 and 2.09 ± 0.11 W $m^{-1}$ $K^{-1}$, respectively, and MY surface ice, 1.88 ± 0.13 W $m^{-1}$ $K^{-1}$, are all consistent with effective medium predictions for measured salinity, density, and temperature. In contrast with a previous result from thermistor array measurements in FY ice, the present measurements in FY ice show no conductivity reduction over the top 50 cm. We have reexamined the analysis of these previous array measurements and have identified analytical effects that rendered this analysis unreliable in the presence of high-frequency surface temperature variations and pronounced surface warming and cooling events. We conclude that this apparent near-surface conductivity reduction was an artefact.

**Citation:** Pringle, D. J., H. J. Trodahl, and T. G. Haskell (2006), Direct measurement of sea ice thermal conductivity: No surface reduction, *J. Geophys. Res.*, *111*, C05020, doi:10.1029/2005JC002990.

## 1. Introduction

[2] Sea ice is an important component in the world climate system because of its extent and its coupling between ocean and atmosphere. Through numerous feedback mechanisms sea ice acts as both an indicator and agent of climate change [e.g., *Eicken and Lemke*, 2001; *Dieckmann and Hellmer*, 2003]. Accurate representations of sea ice processes and properties are important to improve the predictive accuracy of both sea ice models and general circulation models. Both mechanical and thermodynamical aspects are important here. Key thermodynamic parameters are the albedo, heat capacity and thermal conductivity, and it is important that their parameterizations in models are observationally supported. The effect of surface conditions (melt ponds, leads, snow and bare ice) on area-averaged albedo is an area of active research [e.g., *Eicken et al.*, 2004]. The heat capacity is an equilibrium property for which the predictions of theoretical models are in good agreement with experimental values [*Schwerdtfeger*, 1963; *Ono*, 1967; *Johnson*, 1989]. The thermal conductivity $k_{si}$ controls the thermodynamic accretion rate, equilibrium thickness and conductive heat flux through the ice. It has proven difficult to measure, and departures from the expected behavior have been observed including an anomalous near-surface reduction [*Trodahl et al.*, 2001].

[3] Most major sea ice models (including the Los Alamos Sea Ice Model (CICE), National Center of Atmospheric Research (NCAR) Community Atmosphere Model (CAM2), Community Climate System Model (CCSM3.0), Canadian Ice Service Community Ice-Ocean Model (CIOM)) use the conductivity parameterization used in the seminal one-dimensional (1-D) thermodynamic sea ice model of *Maykut and Untersteiner* [1971], $k(S, T) = 2.03 + 0.117\,S/T$, where $S$ is salinity [ppt], $T$ is temperature [°C], and $k$ has units W $m^{-1}$ $K^{-1}$. This formula applies below the salinity-dependent freezing point so involves no discontinuity at $T = 0$. Other models use only the constant term from this expression [e.g., *Parkinson and Washington*, 1979; *Lemke et al.*, 1990; *Wu et al.*, 1997]. This parameterization derives from that of *Untersteiner* [1961], itself predating almost all theoretical and experimental results for $k_{si}$.

[4] Because of the contrast in conductivity of the ice, brine and air components $k_{si}$ is a function of their relative volume fractions and their geometric arrangement. Assuming thermal equilibrium composition, effective medium models can be used to predict the density, salinity and temperature dependence of the conductivity for a prescribed geometry [*Anderson*, 1958; *Schwerdtfeger*, 1963; *Ono*, 1967; *Yen*, 1981]. The largest source of uncertainty in these effective medium models is the conductivity of fresh ice at 0°C (at atmospheric pressure). Measured values range between 2.09 and 2.26 W $m^{-1}$ $K^{-1}$ [*Fukusako*, 1990; *Yen et al.*, 1991], with a best estimate of 2.14 W $m^{-1}$ $K^{-1}$ [*Slack*, 1980].

[5] Compared with the analogous measurement of electrical conductivity, in which confining an electrical current to a sample is readily achieved, the much smaller conductivity contrast between good and poor thermal conductors makes thermal conductivity measurements particularly difficult, especially for low-conductivity materials. For both

[1]School of Chemical and Physical Sciences, Victoria University of Wellington, Wellington, New Zealand.
[2]Arctic Region Supercomputing Center and Geophysical Institute, University of Alaska Fairbanks, Fairbanks, Alaska, USA.
[3]Industrial Research Limited, Lower Hutt, New Zealand.

Copyright 2006 by the American Geophysical Union.
0148-0227/06/2005JC002990$09.00

fresh and sea ice, methods must be chosen that avoid local melting and changes to the internal structure.

[6] Previous experimental determinations of $k_{si}$ can be divided into two categories: the analysis of in situ ice temperatures measured with thermistor or thermocouple arrays, and laboratory measurements (on either natural or artificial samples) [*Malmgren*, 1927; *Schwerdtfeger*, 1963; *Nazintsev*, 1964; *Ono*, 1965; *Lewis*, 1967; *Weller*, 1967]. The thermal array approach is attractive because the measurement is made in largely unperturbed ice, under conditions of natural temperatures and heat flow. However, calculating the conductivity from the temperature record is complicated both in terms of the temperature inversion, and because of the potential of perturbing the local heat flow.

[7] Various analysis methods have been applied to such ice temperatures measurements [e.g., *Malmgren*, 1927; *Lewis*, 1967; *Weller*, 1967] prior to the recent work of our group [*McGuinness et al.*, 1998; *Trodahl et al.*, 2000, 2001]. In situ ice temperatures were recorded through the Austral winter in landfast first-year sea ice in McMurdo Sound, Antarctica, using vertical thermistor arrays designed to minimize the thermal perturbation and high-precision custom-built data loggers. From a conservation of energy analysis (see below) these constitute the most comprehensive measurements of $k_{si}$ to date. These results showed departures from the behavior predicted by effective medium models in that the conductivity of congelation ice ($z > 30$ cm) was about 10% lower than predicted [*Trodahl et al.*, 2000, 2001] and there was a systematic near-surface conductivity reduction of up to ~25% over the top ~50 cm which was most pronounced closest to the surface [*Trodahl et al.*, 2001].

[8] It was proposed that both the overall reduction and the surface effect might be caused by an enhanced scattering of phonons (lattice vibrations responsible for heat conduction in electrical insulators) due to small crystal size particularly in the upper frazil ice layer [*Trodahl et al.*, 2001]. This effect indeed applies when the phonon mean free path, which increases with decreasing temperature, becomes comparable with the crystal dimensions causing a low-temperature conductivity reduction [*Ashcroft and Mermin*, 1976; *Slack*, 1980]. The surface reduction in $k_{si}$ has been met with some scepticism. In fact historical results show a range of behaviors near the surface. The near-surface values of *Malmgren* [1927] are about 50% lower than those predicted by effective medium models, those of *Nazintsev* [1964] (results reported by *Doronin and Kheisin* [1977]) and *Weller* [1967] are about 20% lower, whereas those of *Lewis* [1967] are approximately 15% higher. The work presented here was designed to reexamine this near-surface behavior with direct measurements.

[9] The paper is arranged as follows. We describe our laboratory-based parallel conductance measurements, including equipment and analysis, and compare our results against effective medium predictions. We then describe analytical effects that contributed to the apparent near-surface conductivity reduction in the earlier array measurements, and summarize our results.

## 2. Laboratory Measurements

[10] Conceptually, the thermal conductivity $k$ can be measured directly in a 1-D experiment as the ratio of an applied heat flux $J_Q$ to the resulting temperature gradient, according to Fourier's Law, $J_Q = -kdT/dz$. Conductive and convective heat loss from a sample can be minimized by performing the measurement under high vacuum. However, this approach is problematic for high vapor pressure materials such as ice ($P_v(-10°C) = 7 \times 10^{-3}$ bar) which cannot therefore be held at the required vacuum. To avoid this problem we have used a parallel conductance method. This is a standard approach that permits the accommodation of heat losses that are difficult to determine absolutely [e.g., *Zawilski et al.*, 2001].

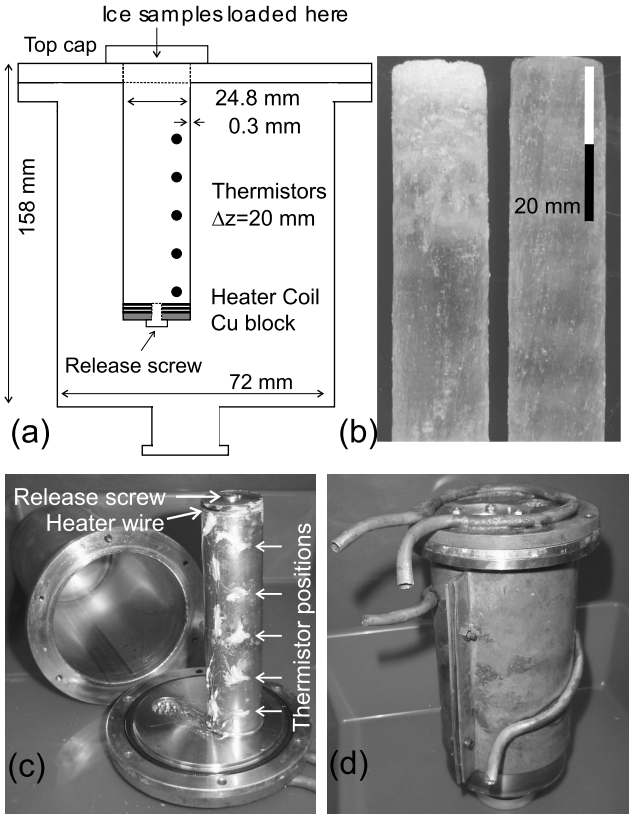


**Figure 1.** (a) Schematic diagram of sample holder protruding into the vacuum chamber. (b) FY core examples for (left) surface ice (0–10 cm) and (right) subsurface ice (45–55 cm). Helical striations are due to coring. (c) Opened chamber showing sample holder tube attached to top flange. Heater wire is wound under the copper base; O-ring sealed release screw is indicated. Thermistor beads were held in place with white high-vacuum epoxy Torr Seal. (d) Copper cladding and tubes on the outside of the chamber through which temperature-controlled fluid was pumped. Note different scales in all figures.

[11] Our measurements were performed in a field laboratory at McMurdo Sound Antarctica, November 2003. Small sea ice cores (~100 × 24 mm diameter) were placed in a cylindrical sample holder tube with a vacuum seal at one end. This tube was mounted on the upper flange of a vacuum chamber with the tube protruding into the chamber. See Figure 1. Heat was supplied with an ohmic heater at the base of the tube inside the chamber, and the temperature profile resulting from heat conduction along the tube was measured with thermistors. The conductivity of individual

ice samples was determined from the measurements with and without a sample in place, assuming parallel heat flow along the holder and sample.

[12] Measurements on extracted cores do admit the possibility of altering the ice through brine drainage, but for temperatures at which our array measurements resolved a conductivity reduction ($T \leq -20°C$) this is not expected to be a problem because the brine volume fraction and permeability are below the percolation limit [*Buckley and Trodahl*, 1987; *Golden et al.*, 1998; *Freitag and Eicken*, 2003]. Cores were never raised above this limit ($-5°C$) and the temperature difference along the cores did not exceed 4°C.

### 2.1. Equipment

[13] A schematic diagram and photographs of the equipment are shown in Figure 1. The sample was contained in a thin-walled (0.3 mm) 304 stainless steel tube with 25.4 mm outside diameter and a welded cap completing the vacuum seal. A copper bobbin fixed to its base was wound with approximately 10 m of constantan wire to make the resistive heater, which was powered with a calibrated Yokogawa 7651 precision current supply. Five YSI 55031 thermistors were positioned approximately 20 mm apart down the sample holder. Care was taken to ensure direct contact between the tube and the center of the thermistor beads. Four-point measurements of thermistor resistances were made with an HP3478A multimeter, with an excitation current of 10 μA causing negligible thermistor self heating. The thermistors were calibrated to a relative accuracy of approximately 0.003°C. The chamber temperature was held constant by pumping a 40/40/20 mixture of ethylene glycol/water/isopropyl alcohol through copper fittings clamped around the chamber, and by housing this arrangement in a well-insulated enclosure (not shown). See Figure 1d.

[14] This approach requires high-vacuum materials for all parts inside the chamber. The sample holder stainless steel has a conductivity $k_{ss}(-10°C) \approx 15$ W m$^{-1}$ K$^{-1}$, about 7 times that of ice but a total conductance (area-weighted conductivity) less than half that of an ice sample.

[15] Thermal contact between the ice and tube was optimized by applying a thin layer of silicone vacuum grease to the inside of the tube before loading each core which then fit tightly into the tube. A cap at the top of the sample holder thermally anchored the top of the sample to the temperature-controlled chamber top. The temperature gradient was measured halfway between the heater and chamber top, where the assumption of parallel heat flow is most robust, and the temperature gradient was monitored over time until a steady state was reached. In the no-ice measurements an O-ring sealed release screw in the base of the tube was removed and the sample space was evacuated with the top cap maintaining the vacuum seal.

### 2.2. Calculating the Conductivity

[16] In the ideal no-loss case, and with no ice core in place, all of the power $P$ dissipated in the heater is conducted up the sample holder and the conductance $K$ of the sample holder tube of length $L$ is given by

$$K = \frac{P}{L\left|\frac{dT}{dz}\right|}. \quad (1)$$

Assuming parallel heat flow, adding an ice sample increases the total conductance $K'$ by the conductance of the ice. The ice conductivity is then given by the change in conductance,

$$k_{ice} = \frac{L}{A}(K' - K), \quad (2)$$

where $A$ is the ice cross sectional area.

[17] At operating chamber pressures of $1-3 \times 10^{-9}$ bar, convective and conductive heat loss from the sample holder to the inside chamber wall are negligible (~0.1% of the applied power). However, radiative losses cannot be eliminated. The decrease in conductive flux along the tube reduces the temperature gradient from what it would otherwise be and equation (1) returns an "apparent thermal conductance" that overestimates the actual conductance. We have modelled radiative losses in our chamber which depend on the emissivity and temperature distribution of the inside chamber wall (see Appendix). These conditions are the same whether an ice sample is loaded or not, so that to a very good approximation adding an ice sample increases the "apparent conductance" by the actual conductance of the ice. Therefore the conductivity of a sample can still be found with the same subtraction procedure using equation (1) by taking the difference in the measured "apparent conductance" with and without a sample in place.

[18] We estimate an uncertainty in this approach (~± 2%) that is less than the experimental uncertainties derived from variations in thermal contact and intrinsic sample properties, and from the temperature gradient measurement. Note that although constant for identical chamber conditions, the emissivity and temperature distribution of the chamber are not sufficiently well constrained to permit a direct absolute measurement of the conductivity of the tube itself.

[19] For typical measurements with an ice sample in place, a heater power of 67 mW induced a temperature gradient of approximately −40°C/m, corresponding to radiative losses of about 15%. The maximum calculated change in brine volume fraction was from approximately 5% at the base of the sample to 3% at the top. This difference was reduced over the 40 mm for which the conductivity was calculated where the predicted conductivity variation due to the salinity and temperature gradients is small (0.03 W m$^{-1}$ K$^{-1}$). As this variation is approximately linear with distance along the tube it does not affect the conductivity calculated from the average temperature gradient measured at the center of this region.

### 2.3. Results for First-Year and Multiyear Landfast Antarctic Sea Ice

[20] Measurements were made on cores (~100 × 24 mm diameter) drilled from landfast first-year (FY) and multiyear (MY) McMurdo Sound sea ice. Blocks of ice approximately 45 cm on a side were cut from the surface (0–45 cm) and subsurface (45–90 cm) at a FY site near where previous thermal array measurements were made (S 77°43′; E 166°26′), and from the surface of MY ice off Arrival Heights near a recently installed array site (S 77°50′, E 166°37′). Several cores of each type were extracted from these blocks using a custom-built coring unit and stored in air tight bags at −18°C to prevent brine drainage. Density and salinity values from measurements on several cores in

**Table 1.** Characterization of Ice Types and Comparison of Measured and Predicted Thermal Conductivities[a]

| Ice Type/Depth, cm | Density, g/cm$^3$ | Salinity, ppt | $T$, °C | $k$ (Measured), W m$^{-1}$ K$^{-1}$ | $k$ (Predicted), W m$^{-1}$ K$^{-1}$ |
|---|---|---|---|---|---|
| FY 0–10 | 0.90 ± 0.01 | 5.3 ± 0.2 | −9.4 | 2.14 ± 0.11 | 2.11 ± 0.04 |
| FY 45–55 | 0.92 ± 0.01 | 4.5 ± 0.2 | −11.0 | 2.09 ± 0.11 | 2.21 ± 0.04 |
| | | | −10.5[b] | 2.16 ± 0.13 | 2.20 ± 0.04 |
| MY 0–10 | 0.82 ± 0.01 | 0.2 ± 0.2 | −13.0 | 1.88 ± 0.13 | 1.94 ± 0.04 |

[a]Predicted values are from the parallel heat flow model of *Schwerdtfeger* [1963] with updated ice, brine and air conductivities. $T$ is the average temperature over measurements for each ice type listed in Table 2.
[b]Outlier is omitted for these values.

each ice type are collated in Table 1. The FY ice is typical of the ice in which thermal array measurements were made at nearby sites in previous years.

[21] The apparent thermal conductance of the tube was measured with heater powers in the range 17–67 mW, and chamber temperatures −9.5°C and −15.0°C. The average apparent conductance over this temperature range was ($\overline{K}_{app}$ = 8.76 ± 0.23 mW/K). Ice sample measurements were made at these two chamber temperatures with heater powers of 34, 49, 67 mW.

[22] Conductivity results found from the difference in apparent conductance of the sample and tube-only measurements are listed in Table 2 for the 4 surface and 3 subsurface FY ice cores, and 2 surface MY cores. These values represent the conductivity halfway along the sample holder where the temperature gradients were measured. They are plotted against the temperature at this point in Figure 2 in which effective medium predictions are also shown. The predicted values have been calculated with the parallel component "bubbly ice" and brine conductivity model of *Schwerdtfeger* [1963] updated with the fresh ice conductivity of *Slack* [1980] and other component conductivities from *Yen* [1981]. Upper and lower bounds are shown for the uncertainty in density and salinity for each ice type. Thirteen of the fifteen measurements overlap the predicted values and Figure 2 clearly illustrates that the difference in individual FY surface and subsurface conductivity values is below the resolution of these measurements. The FY subsurface results are consistent with conductivity values from array measurements at depths below 50 cm which are not affected by the near-surface reduction.

[23] The dash-dotted curve shows the *Maykut and Untersteiner* [1971] prediction for $S$ = 5 ppt. A full comparison of this representation with the present results, array results from our amended analysis and historical measurements will be presented elsewhere (D. J. Pringle et al., Thermal conductivity of landfast Antarctic and Arctic sea ice, submitted to Journal of Geophysical Research, 2006, hereinafter referred to as Pringle et al., submitted manuscript, 2006). In that paper we discuss an alternative representation to account for the density, temperature and salinity dependence of $k_{si}$. For now we just note that compared with the FY results, this prediction is lower than all but the one low-lying subsurface measurement.

[24] Ice-type averages are also compared with predictions for the average measurement temperature in Table 1. The good comparison is made even better if one outlying FY subsurface value (1.90 ± 0.15 W m$^{-1}$ K$^{-1}$) is rejected, changing that ice-type average to 2.16 ± 0.13 W m$^{-1}$ K$^{-1}$.

**Table 2.** Measured Conductivity Values for FY Surface (0–10 cm), FY Subsurface (45–55 cm), and MY Surface (0–10 cm) Ice[a]

| Core | $T$, °C | Measured $k$, W m$^{-1}$ K$^{-1}$ | Predicted $k$, W m$^{-1}$ K$^{-1}$ |
|---|---|---|---|
| S-1 | −7.67 | 2.31 ± 0.22 | 2.08 ± 0.04 |
| S-2 | −7.55 | 2.21 ± 0.23 | 2.08 ± 0.04 |
| S-2 | −8.55 | 2.18 ± 0.23 | 2.10 ± 0.04 |
| S-3 | −7.40 | 2.04 ± 0.19 | 2.08 ± 0.04 |
| S-3 | −8.44 | 2.12 ± 0.18 | 2.10 ± 0.04 |
| S-4 | −13.64 | 2.07 ± 0.20 | 2.18 ± 0.04 |
| S-4 | −12.51 | 2.16 ± 0.22 | 2.16 ± 0.04 |
| FY-s | −9.40 | 2.14 ± 0.11 | 2.11 ± 0.04 |
| SS-1 | −13.17 | 2.23 ± 0.34 | 2.24 ± 0.04 |
| SS-2 | −8.20 | 2.08 ± 0.22 | 2.17 ± 0.04 |
| SS-2 | −7.14 | 2.24 ± 0.21 | 2.15 ± 0.04 |
| SS-3 | −13.76 | 1.90 ± 0.18 | 2.25 ± 0.04 |
| SS-3 | −12.71 | 2.13 ± 0.19 | 2.24 ± 0.04 |
| FY-ss | −11 | 2.09 ± 0.12 | 2.21 ± 0.04 |
| MY-1 | −12.65 | 1.78 ± 0.20 | 1.94 ± 0.03 |
| MY-1 | −13.31 | 1.73 ± 0.17 | 1.95 ± 0.03 |
| MY-2 | −13.19 | 2.10 ± 0.19 | 1.95 ± 0.03 |
| MY-s | −13.05 | 1.88 ± 0.13 | 1.94 ± 0.03 |

[a]Uncertainties in individual measured conductivity values include both systematic and random uncertainties. The last line for each ice type gives the weighted average conductivity and the predicted conductivity for the average temperature. Predicted values are for the *Schwerdtfeger* [1963] model of "bubbly ice" and brine in parallel.

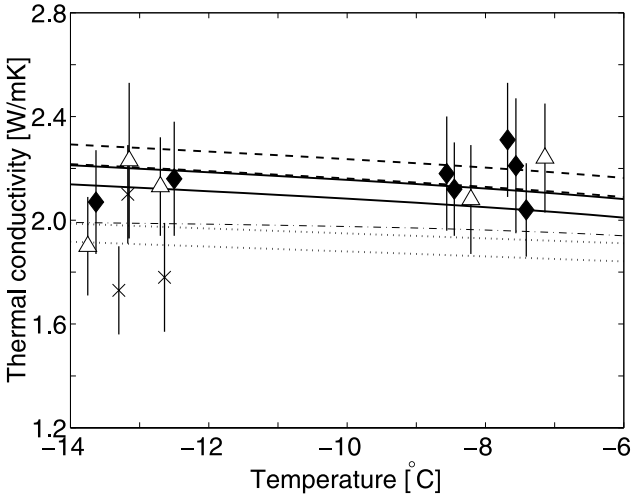


**Figure 2.** Experimental conductivity results (symbols) and predicted values (lines): FY surface ice, solid diamonds and solid lines; FY subsurface ice, open triangles and dashed lines; MY surface ice, crosses and dotted lines. Predictions are from the updated parallel heat flow model of *Schwerdtfeger* [1963]. The two lines for each ice type indicate the range in predictions derived from salinity and density uncertainties. The dash-dotted line near the top MY line is the representation of *Maykut and Untersteiner* [1971], $k$ = 2.03 + 0.117 $S/T$ for $S$ = 5 ppt.

[25] These measurements reproduce the thermal conductivities of both the effective medium model and the thermal array measurements at depths where they are reliable. They do not show an anomalous near-surface reduction although they do resolve the density-dependent reduction predicted for the bubbly MY ice which is approximately a factor of 2 smaller than the previously reported near-surface reduction.

## 3. Reexamining Analysis of Array Measurements

[26] The results of laboratory experiments discussed in the preceding section are in clear disagreement with the near-surface reduction generated by the earlier analysis of array measurements, so we have repeated and examined the indirect array determination to seek an understanding of the source of the underestimated values. Conductivity values from an amended analysis of both new and previously reported temperature measurements are to be presented elsewhere (Pringle et al., submitted manuscript, 2006). Here we discuss aspects of the analysis relevant to the near-surface reduction. Earlier data have already been described fully [*McGuinness et al.*, 1998; *Trodahl et al.*, 2000, 2001], and additional new measurements have been performed in landfast Antarctic (FY and MY) and Arctic (FY) ice. Internal ice temperatures were measured every $\Delta t = 30$ min at vertical intervals of $\Delta z = 10$ cm. All array measurements were performed during the Austral winter so solar heating of the ice or thermistor arrays cannot be responsible for the near-surface apparent conductivity reduction.

[27] The array data were analyzed assuming 1-D heat conduction with no heat sinks or sources in the ice, using a conservation of energy analysis according to which [*Trodahl et al.*, 2000]

$$\rho \partial_t U = k \partial_{zz} T. \tag{3}$$

Here $\rho$ is the sea ice density, and $U(T, S)$ the sea ice internal energy per unit mass found by integrating the theoretical result for the heat capacity of *Ono* [1967]. Finite difference estimates of the derivatives were made according to $\partial_t U = (U(t + \Delta t) - U(t - \Delta t))/2\Delta t$, and $\partial_{zz} T = (T(z + \Delta z) - 2T(z) + T(z - \Delta z))/\Delta z^2$. The conductivity was determined as the best fit gradient of scatterplots of $\rho \partial_t U$ versus $\partial_{zz} T$. Three thermistors are required to estimate $\partial_{zz} T$, so this analysis gives the average apparent conductivity over this three-thermistor interval, $2\Delta z = 20$ cm. A conductivity profile was determined by applying the analysis down the thermistor chain.

[28] We now discuss a number of potential sources for the apparent surface reduction generated by these measurements and analysis. Three are of sufficient importance and require such detail that they have been assigned their own sections below, but we start with two that, while potentially problematic, are unlikely to lead to the systematic reduction. First there is the question as to whether the array, with its somewhat different heat conduction characteristics, might bias the measurements. This issue was thoroughly discussed in an earlier publication [*Trodahl et al.*, 2000] and shown to be of negligible importance on the basis of the relatively close match between the thermal conductance of the probe and of the ice it replaces. Although the conductivity of stainless steel is higher than that of ice, the cross sectional area contrast more than compensates for that higher conductivity. The probe design further permits that the hole required for deployment has a very small diameter, so that even the volume of refrozen seawater filling the hole has minimal dimensions. Revisiting the question has brought no new conclusions in that regard, and we have no reason to suspect that the probe causes significant disturbance. Secondly, *Sturm et al.* [2002] discussed departures from 1-D heat flow in ridged ice with an uneven snow cover. The upper ice surface at our landfast McMurdo Sound sites was very flat, so there is no reason to doubt the validity of our 1-D model. Furthermore the effect would be expected to lead to departures of both signs, both increases and decreases, while we consistently found only a reduction near the surface.

[29] We now examine three more serious problems: the effect of the omission in equation (3) of a term relating to the depth derivative of the conductivity, the effect of a transcription error in the equation giving the temperature-dependent heat capacity, and finally the effect of high-frequency temperature variations on the accuracy of our analysis.

### 3.1. Omission of Conductivity Depth Dependence in Heat Equation

[30] The analysis above assumes a locally constant conductivity ($\partial k/\partial z = 0$), and therefore returns an average conductivity for each three-thermistor interval. Without this assumption the heat equation includes a further term proportional to the derivative of the conductivity, giving

$$\rho \partial_t U = k \partial_{zz} T + \frac{\partial k}{\partial z} \frac{\partial T}{\partial z}. \tag{4}$$

[31] We have evaluated the omitted term and, using a similar method as before, determined the conductivity as the gradient of scatter plots of $(\rho \partial_t U - \frac{\partial k}{\partial z}\frac{\partial T}{\partial z})$ versus $\partial_{zz} T$.

[32] The omitted term can be expanded as

$$\frac{\partial k}{\partial z}\frac{\partial T}{\partial z} = \left[\frac{\partial k}{\partial T}\frac{\partial T}{\partial z} + \frac{\partial k}{\partial S}\frac{\partial S}{\partial z} + \frac{\partial k}{\partial \rho}\frac{\partial \rho}{\partial z}\right]\frac{\partial T}{\partial z}, \tag{5}$$

where the terms on the RHS of this expression are in order of decreasing magnitude. We have calculated the spatial derivatives $\partial T/\partial z$ and $\partial S/\partial z$ from measured temperature and salinity profiles, and the conductivity derivatives using the effective medium model of *Schwerdtfeger* [1963]. For winter temperatures the previously omitted term lies in the range $-6$ to 0 W/m$^3$, with fluctuations about an average value determined by the relatively slowly varying average temperature gradient. The correction term increases slightly with increasing rate of cooling ($\partial_t U < 0$) so that its inclusion actually decreases the near-surface conductivity by about 1–2%, which is less than the array measurement accuracy. The omission of this term did not contribute to the near-surface reduction.

### 3.2. Correction to Heat Capacity

[33] In the earlier analysis there was an error in the heat capacity expression integrated to find the internal energy

$U(T, S)$. In units of [J/gK] the result of *Ono* [1967] should read

$$c_{si} = 2.113 + 0.0075\,T - 0.0034\,S + 0.00008\,ST + 18.04\,\frac{S}{T^2}, \quad (6)$$

for $S$ [ppt] and $T$ [°C], but in the review articles of *Yen* [1981] and *Yen et al.* [1991] the coefficient of the fourth term is mistakenly written 0.0008 *ST*.

[34] This error led to an underestimation of the magnitude of $\rho\partial_t U$ values and therefore the conductivity. Both the temperature and salinity profiles (bulk values of 5–6 ppt increasing to 8–10 ppt near the surface) at these sites result in this error increasing toward the ice surface where wintertime surface temperatures were typically below −20°C. For $S$ = 6, the conductivity reduction at $T$ = −10°C and −25°C, is 1% and 5%, respectively. This accounts for a small though not insignificant fraction of the near-surface reduction.

### 3.3. Rapid Temperature Fluctuations

[35] Our finite difference estimates are reliable when the sampling intervals are small compared with the time and length scale of the temperature variations, that is, $\omega\Delta t < 1$, and $\Delta z < d$, where $d = (2D/\omega)^{1/2}$ is the penetration depth for frequency $\omega$ and thermal diffusivity $D$. These conditions are not met for short-penetration depth rapid fluctuations in the surface temperature which can lead to an underestimation of the conductivity as follows.

[36] The linear least squares fitting procedure underestimates the gradient when there are errors in the variable treated as independent (the $x$ axis variable) [*Fuller*, 1987]. In our case there are errors in both plotted variables and we have calculated the conductivity as the geometric mean of gradient estimates first treating $\partial_{zz}T$ and then $\rho\partial_t U$ as the independent variable [*McGuinness et al.*, 1998; *Trodahl et al.*, 2000]. This gives an unbiased estimate when the relative errors are the same in both variables but one that is biased downward if the relative uncertainties in $\partial_{zz}T$ are larger than those in $\rho\partial_t U$ [*Fuller*, 1987].

[37] Temperature variations for which $d < \Delta z$ introduce a high-frequency component in $\partial_{zz}T$, which is calculated from temperatures at three successive depths, that does not appear in $\rho\partial_t U$ calculated at the central thermistor. This increased scatter in $\partial_{zz}T$ values constitutes an increase in its relative error, and biases the geometric mean conductivity to lower values.

[38] A near-surface conductivity reduction under these circumstances has been confirmed by analyzing simulated temperatures. Heat conduction through a growing or decaying ice sheet has a transcendental solution due to the moving lower-boundary condition [e.g., *Wettlaufer*, 2001], but the near-surface response can be approximated by harmonic driving of a uniform half-space. We analyzed simulated temperatures including some components not satisfying $\omega\Delta t < 1$, $\Delta z < d$ and sampled these temperatures at the original array measurement intervals $\Delta z$ = 10 cm and $\Delta t$ = 1 hr, including a realistic measurement noise and precision. Figure 3a shows the analyzed temperatures and Figure 3b the resulting scatterplots for thermistors at depths of 15 and 25 cm in which a broadening of the 15 cm scatterplot is particularly clear. Figure 3c shows the near-surface reduction in the resulting conductivity profile. This reduction was largely removed by low-pass filtering the sampled temperatures prior to the finite difference analysis. See Figures 3d and 3e.

[39] Rapid temperature fluctuations also give rise to loops in the scatterplots, as seen in field measurements, which are associated with a conductivity reduction too. Figure 4a shows an example of these loops which were previously described by *Trodahl et al.* [2000]. The loops are traced out counterclockwise indicating a time lag between the $\rho\partial_t U$ and $\partial_{zz}T$ estimates, as expected for high-frequency driving (see Appendix A). Figure 4b illustrates a loop formed by a single harmonic temperature component. The ideal behavior is shown by the dashed line. Both the broadening and downward tilt in principle direction of this loop serve to lower the calculated conductivity. Figure 4c illustrates the result for two-component driving. Points derived from the lower-frequency component show a local gradient that is accurate, but the effect of the high-frequency component is to spread out laterally these subsets of points which decreases the calculated conductivity.

[40] Our field data show prominent loops and a strong conductivity reduction for the shallow thermistors at times of pronounced surface temperature change (variations at $z$ = 5 cm up to ∼15°C over 2 days). These episodes are associated with large values of $\rho\partial_t U$ and $\partial_{zz}T$, so they strongly influence the fitted gradient for scatterplots from any time period including these events. Temperatures from these time periods are now excluded from our analysis.

[41] A loss of accuracy in our finite difference derivative estimates in the presence of rapid temperature fluctuations was the largest contributing factor in the apparent near-surface conductivity reduction. Further to correcting the heat capacity error, by low-pass filtering measured temperatures and excluding temperatures from pronounced surface temperature episodes, this near-surface reduction is removed.

## 4. Summary and Conclusions

[42] This work was designed to reexamine an anomalous near-surface reduction in thermal array measurements of the thermal conductivity $k_{si}$ of FY sea ice. We have described and presented results from a laboratory-based parallel conductance measurement of the thermal conductivity of small natural sea ice cores. The conductivity of these cores was measured from the change in conductance of a thin-walled stainless steel tube when an ice sample was loaded. The subtraction procedure accounts for both conduction up the tube and radiative losses. The conductivities for surface (0–10 cm) and subsurface (45–55 cm) FY ice, 2.14 ± 0.11 and 2.09 ± 0.11 W m$^{-1}$ K$^{-1}$, respectively, and MY surface ice (0–10 cm), 1.88 ± 0.13 W m$^{-1}$ K$^{-1}$, are all consistent with effective medium predictions for ice-type average salinity, density and temperature, and with thermistor array measurements at depths where those measurements are reliable. In contrast with the previous array measurements the present measurements show no significant difference in the conductivity of the surface and subsurface FY ice and certainly no large reduction over the top 50 cm [*Trodahl et al.*, 2001]. Measurements were made between −7° and −14°C

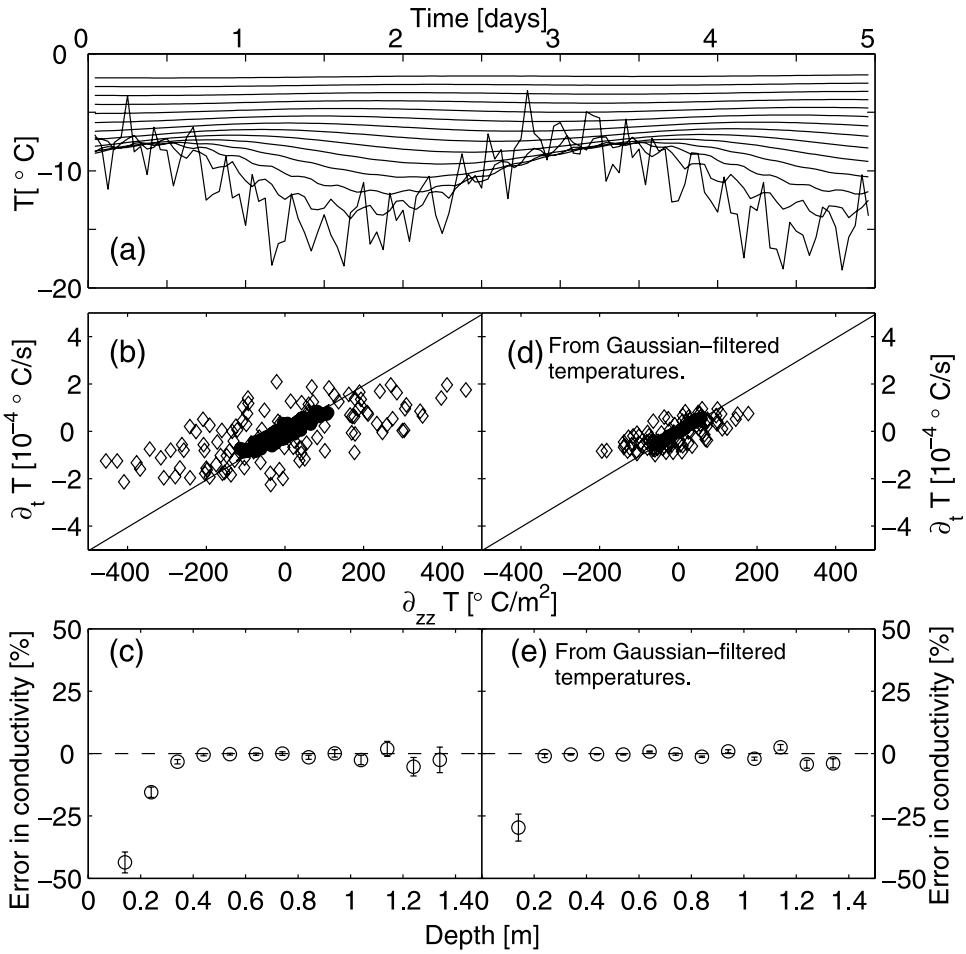


**Figure 3.** Analysis of simulated temperatures including Gaussian noise ($\sigma_T$ = 0.002°C) and finite temperature resolution ($\delta T$ = 0.001°C). (a) Simulated temperatures, sampled with $\Delta z$ = 10 cm and $\Delta t$ = 1 hour. (b) Scatterplots derived from the above temperatures, at $z$ = 15 and 25 cm (open diamonds, solid circles, respectively). The line shows ideal behavior. (c) Near-surface conductivity reduction due to sampling interval effects. (d, e) As for Figures 3b and 3c but after time domain filtering with a Gaussian window of width 1 day and power spectrum half height of 12 hours. Departures from expected conductivity below 1 m in Figures 3d and 3e occur as the analysis becomes noise limited at depths where the temperature variations are weak.

although the intrinsic temperature dependence of $k_{si}$ was below our resolution.

[43] From a reexamination of our earlier analysis of thermistor array measurements we have identified analytical effects that rendered this analysis unreliable in the presence of high-frequency surface temperature variations and pronounced surface warming and cooling events. We determined the conductivity as the best fit gradient to scatterplots of $\rho\partial_t U$ versus $\partial_{zz}T$. There are uncertainties in both plotted variables and the conductivity was calculated as the geometric mean of the least squares gradients found by treating each variable as the independent variable. The accuracy of our finite difference estimates of $\partial_t U$ and $\partial_{zz}T$ is compromised by high-frequency temperature variations near the surface, leading to a decrease in the geometric mean conductivity which is biased by the difference in relative errors in the plotted variables. First, high-frequency temperature components, with a penetration depth less than the thermistor spacing $\Delta z$, introduce a larger relative uncertainty in the $\partial_{zz}T$ estimates than in the $\rho\partial_t U$ estimates. In addition, finite sampling intervals led to loops in these scatterplots due to a time lag between the $\rho\partial_t U$ and $\partial_{zz}T$ estimates. Rather than simply scattering points evenly about a line of slope $k$, these loops are both offset along and tilted toward the $\partial_{zz}T$ axis, and both effects result in a lower computed conductivity. The analysis of simulated temperatures confirmed that these effects lead to a near-surface conductivity reduction. In addition, a transcription error in the heat capacity contributed a conductivity decrease that increased with decreasing temperature and increasing salinity, and therefore toward the surface at our sites. For typical values $S$ = 6 ppt and $T$ = −20°C this produced a 5% reduction in the conductivity.

[44] The omission of the conductivity depth dependence ($\partial k/\partial z$) in the array analysis did not contribute to the near-surface reduction. For temperatures measured in the Austral winter there are no complications from solar heating of either the array or ice. There is only a small thermal

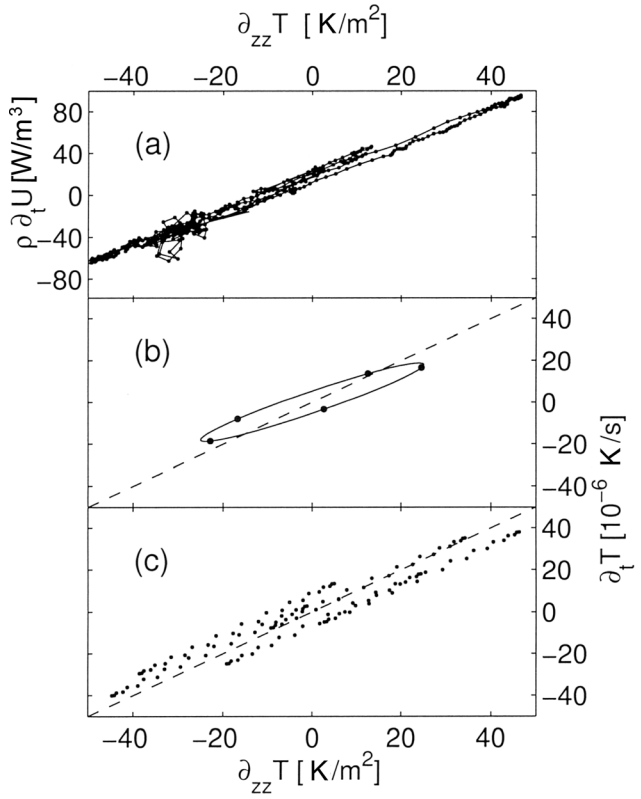


**Figure 4.** (a) Loops in experimental scatterplot for $z$ = 25 cm, from 10 days' data in landfast FY McMurdo Sound ice, 1999. (b, c) Loops from analyzing simulated temperatures with sampling intervals $\Delta z = 0.1$ m and $\Delta t = 30$ min. Figure 4b shows single-component surface temperature driving of 1°C amplitude, for a 5 hour period. Points from finite difference analysis of simulated temperatures and lines show predicted behavior from equations (A5) and (A8). Figure 4c shows two-component driving, 1°C amplitude for 5 and 24 hour periods. Loops are omitted for clarity. In Figures 4b and 4c, points ideally should lie on the dashed lines, whose slope gives the diffusivity $D = 1 \times 10^{-6}$ m$^2$/s, here proportional to the conductivity.

mismatch between the small diameter arrays and the ice it displaces which is not considered to have biased the measurements.

[45] Conductivity results from an amended analysis of new and previously analyzed array measurements in landfast Antarctic (FY and MY) and Arctic (FY) ice will be published separately. Results from arrays of the design described here and arrays in which thermistors were housed in fingers extending from a 20 mm diameter white-painted polycarbonate-polyethylene conduit show no anomalous surface reduction.

## Appendix A: Mathematical Details

[46] We here discuss mathematical aspects of our parallel conductance measurements and the effect of finite sample intervals on our thermistor array analysis.

[47] 1. In the parallel conductance measurements there was a net radiative loss from the sample holder tube to the chamber walls due to their temperature difference. Consider heat flow in the $z$ direction along a homogeneous bar of density $\rho$, specific heat $c$, thermal conductivity $k$, cross sectional area $A$, and circumference $s$. For heat loss to an isothermal surrounding at temperature $T_c$ that is proportional to the excess temperature along the bar $\theta = T - T_c$, the heat equation reads

$$\partial_{zz}\theta = D\partial_t\theta + \alpha^2\theta. \tag{A1}$$

Here $\alpha^2 = (ns/kA)$ where $n$ [W m$^{-2}$ °C] is the heat loss proportionality coefficient and $D = \rho c/k$ is the thermal diffusivity.

[48] In our case $n$ is purely radiative. For a black body radiating into an isothermal background at $T_c$ with a small excess temperature, $n \approx 4\sigma T_c^3$ where $\sigma$ is the Stefan-Boltzmann constant. For our chamber we find $n \approx 3.5\epsilon_{SS}\sigma T_c^3$ where $\epsilon_{SS}$ in the emissivity of stainless steel, and the reduction in prefactor derives from the finite size of the radiating areas [*Winterton*, 1997]. In addition, a small fraction of the heater power $P$ will be lost from the copper heater base of area $A_{Cu}$, given by $\beta \approx 4\sigma\epsilon_{\mathrm{Cu}}T_c^3\,\theta A_{Cu}/P$. The steady state solution to equation (A1) is then

$$\theta(z) = \frac{P(1-\beta)}{\alpha LK}\,\frac{\sinh\,(\alpha L(1-z/L))}{\cosh(\alpha L)}, \tag{A2}$$

where $K = kA/L$ is the thermal conductance.

[49] The apparent thermal conductance evaluated at $z = \frac{L}{2}$ with equations (1) and (A2) is

$$K_{app} = \frac{K}{1-\beta}\,\frac{\cosh(\alpha L)}{\cosh\left(\frac{1}{2}\alpha L\right)}. \tag{A3}$$

In the no-loss case the apparent conductance of the ice is given by $K_{app}(ice) = K_{app}(ice + tube) - K_{app}(tube)$. Evaluating this difference using equation (1) and by expanding equation (A3) to order $(\alpha L)^2$ (introducing an error of at most 0.5%) for the ice and no-ice cases, gives

$$K_{app}(ice) = \frac{1}{1-\beta'}K_{ice} + \left(\frac{1}{1-\beta'} - \frac{1}{1-\beta}\right)K_{tube} + \frac{3sL}{8}\left(\frac{n'}{1-\beta'} - \frac{n}{1-\beta}\right), \tag{A4}$$

where primes refer to the ice sample measurements. $K_{app}(ice)$ is the value we calculate as the change in apparent conductance when an ice sample is loaded, and $K_{ice}$ is the true value. In our measurements $K_{ice} \sim 10$ mW/K, $K_{tube} \sim 5$ mW/K, $\beta \approx 0.02$, $\beta' \approx 0.01$. For our measurements the RHS of equation (A4) gives the true ice conductance $K_{ice}$ to approximately ±2%. Measurement uncertainties are larger than this limiting methodical accuracy.

[50] 2. The effect of finite sampling intervals on the derivative estimates in the thermistor array analysis can be illustrated with the harmonic surface driving of a semi-infinite uniform half-space of diffusivity $D$ and initial temperature $T = 0$. For surface driving $T(0, t) = T_0\cos(\omega t)$, subsurface temperatures are given by $T(z, t) = T_0 e^{-z/d}\cos(\omega t - z/d)$.

[51] Evaluating the finite difference estimates of $\partial_t T$ and $\partial_{zz} T$ using the method of section (3) then gives

$$\partial_t T|_{FD} = \frac{T(z,t+\Delta t) - T(z,t-\Delta t)}{2\Delta t} = -\omega\left(\frac{\sin(\omega\Delta t)}{\omega\Delta t}\right) T_0 e^{-z/d}\sin(\omega t - z/d), \quad \text{(A5)}$$

and, similarly,

$$\partial_{zz} T|_{FD} = \frac{-2}{d^2}\left(a^2+b^2\right)^{1/2} T_0 e^{-z/d} \times \sin\left(\omega t - z/d + \tan^{-1}\left(\frac{b}{a}\right)\right) \quad \text{(A6)}$$

$$a = \frac{\sinh\left(\Delta z\sqrt{\frac{\omega}{2D}}\right)\sin\left(\Delta z\sqrt{\frac{\omega}{2D}}\right)}{(\Delta z)^2\frac{\omega}{2D}} \quad \text{(A7)}$$

$$b = \frac{\cosh\left(\Delta z\sqrt{\frac{\omega}{2D}}\right)\cos\left(\Delta z\sqrt{\frac{\omega}{2D}}\right) - 1}{(\Delta z)^2\frac{\omega}{2D}}. \quad \text{(A8)}$$

Compared with the relevant analytical expressions, $\partial_t T|_{FD}$ (and therefore $\rho\partial_t U \approx \rho c_{si}(T)\partial_t T$) is underestimated by a factor $\mathrm{sinc}(\omega\Delta t)$, and $\partial_{zz} T|_{FD}$ is phase shifted with a small magnitude increase. The phase shift between equations (A5) and (A6) causes Lissajous figures (loops) in plots of $\partial_t T|_{FD}$ versus $\partial_{zz} T|_{FD}$. These are traced once per period in a counterclockwise fashion,as in Figure 4.

[52] **Acknowledgments.** We gratefully acknowledge Hajo Eicken for support at the Geophysical Institute, University of Alaska Fairbanks; Alan Rennie for technical expertise; and Mark McGuinness for helpful discussions. Logistic support in Antarctica was provided by Antarctica New Zealand, and funding was provided by the New Zealand Public Good Science Fund. We thank Bruno Tremblay and three anonymous reviewers who substantially contributed to the improvement of the article.

## References

Anderson, D. L. (1958), A model for determining sea ice properties, in *Arctic Sea Ice, Publ. 598*, pp. 148–152, U. S. Natl. Acad. Sci., Natl. Res. Counc., Washington, D. C.

Ashcroft, N. W., and N. Mermin (1976), *Solid State Physics*, Holt, Rinehart, and Winston, Austin, Tex.

Buckley, R., and H. J. Trodahl (1987), Thermally driven changes in the optical properties of sea ice, *Cold Reg. Sci. Technol.*, *14*, 201–204.

Dieckmann, G. S., and H. H. Hellmer (2003), The importance of sea ice: An overview, in *Sea Ice: An Introduction to its Physics, Biology, Chemistry and Geology*, edited by D. N. Thomas and G. S. Dieckmann, pp. 1–21, Blackwell Sci., Malden, Mass.

Doronin, Y. P., and D. E. Kheisin (1977), *Sea Ice*, translated from Russian, Amerind, New Delhi, India.

Eicken, H., and P. Lemke (2001), The response of polar sea ice to climate variability and change, in *Climate of the 21st Century: Changes and Risks*, edited by J. L. Lozan, pp. 206–211, Wiss. Auswertungen, Hamburg, Germany.

Eicken, H., T. C. Grenfell, D. K. Perovich, J. A. Richter-Menge, and K. Frey (2004), Hydraulic controls of summer Arctic pack ice albedo, *J. Geophys. Res.*, *109*, C08007, doi:10.1029/2003JC001989.

Freitag, J., and H. Eicken (2003), Melt water circulation and permeability of Arctic summer sea ice derived from hydrological field experiments, *J. Glaciol.*, *49*, 349–358.

Fukusako, S. (1990), Thermophysical properties of ice, snow and sea ice, *Int. J. Thermophys.*, *11*(2), 353–373.

Fuller, W. (1987), *Measurement Error Models*, John Wiley, Hoboken, N. J.

Golden, K., S. F. Ackley, and V. I. Lytle (1998), The percolation phase transition in sea ice, *Science*, *282*(5397), 2238–2241, doi:10.1126/science.282.5397.2238.

Johnson, H. L. (1989), The specific heat of sea ice, B.Sc. honors thesis, Victoria Univ. of Wellington, Wellington, New Zealand.

Lemke, P., W. B. Owens, and W. D. Hibler III (1990), A coupled sea ice-mixed layer-pycnocline model for the Weddell Sea, *J. Geophys. Res.*, *95*, 9513–9525.

Lewis, E. L. (1967), Heat flow through winter ice, in *Physics of Snow and Ice: International Conference on Low Temperture Science 1966*, vol. 1, edited by H. Oura, pp. 611–631, Inst. of Low Temp. Sci., Hokkaido Univ., Sapporo, Japan.

Malmgren, F. (1927), On the properties of sea ice, in *The Norwegian North Polar Expedition with the 'Maud' 1918–1925*, vol. 1a, edited by H. U. Sverdrup, pp. 1–67, John Griegs Boktrykkeri, Bergen, Norway.

Maykut, G., and N. Untersteiner (1971), Some results from a time-dependent thermodynamic model of sea ice, *J. Geophys. Res.*, *76*, 1550–1576.

McGuinness, M. J., K. Collins, H. J. Trodahl, and T. G. Haskell (1998), Nonlinear thermal transport and brine convection in first year sea ice, *Ann. Glaciol.*, *27*, 471–476.

Nazintsev, Y. L. (1964), Nekotorye dannye k raschetu teplovykh svoistv morskogo l'da (Some data on the calculation of thermal properties of sea ice), *Tr. Arkt. Antarkt. Inst.*, *267*, 31–47.

Ono, N. (1965), Themal properties of sea ice. I: Measurements of the thermal conductivity of young winter ice (in Japanese with English summary), *Low Temp. Sci., Ser. A*, *23*, 167–176.

Ono, N. (1967), Specific heat and fusion of sea ice, in *Physics of Snow and Ice: International Conference on Low Temperture Science 1966*, vol. 1, edited by H. Oura, pp. 599–610, Inst. of Low Temp. Sci., Hokkaido Univ., Sapporo, Japan.

Parkinson, C., and W. Washington (1979), A large scale numerical model of sea ice, *J. Geophys. Res.*, *84*, 311–337.

Schwerdtfeger, P. (1963), The thermal properties of sea ice, *J. Glaciol.*, *4*, 789–807.

Slack, G. A. (1980), Thermal conductivity of ice, *Phys. Rev. B*, *22*(6), 3065–3071.

Sturm, M., J. Holmgren, and D. K. Perovich (2002), Winter snow cover on the sea ice of the Arctic Ocean at the Surface Heat Budget of the Arctic Ocean (SHEBA): Temporal evolution and spatial variability, *J. Geophys. Res.*, *107*(C10), 8047, doi:10.1029/2000JC000400.

Trodahl, H. J., M. McGuinness, P. Langhorne, K. Collins, A. Pantoja, I. Smith, and T. Haskell (2000), Heat transport in McMurdo Sound first-year fast ice, *J. Geophys. Res.*, *105*, 11,347–11,358.

Trodahl, H. J., S. Wilkinson, M. McGuinness, and T. Haskell (2001), Thermal conductivity of sea ice: Dependence on temperature and depth, *Geophys. Res. Lett.*, *28*, 1279–1282.

Untersteiner, N. (1961), On the mass and heat balance of Arctic sea ice, *Arch. Meteorol. Geophys. Bioklimatol., Ser. A*, *12*, 151–182.

Weller, G. (1967), The effect of absorbed solar radiation on the thermal diffusion in Antarctic fresh-water ice and sea ice, *J. Glaciol.*, *6*, 859–878.

Wettlaufer, J. S. (2001), The Stefan problem: Polar exploration and the mathematics of moving boundaries, in *Die Zentralanstalt für Meteorologie und Geodynamik, 1851–2001, 150 Jahre Meteorologie und Geophysik in Österreich*, edited by C. Hammerl et al., pp. 420–435, Leykam Buchverlagsges., Graz, Austria. (Available at http://earth.geology.yale.edu/~jw378/articles/StefanFinal.pdf.)

Winterton, R. H. S. (1997), *Heat Transfer*, Oxford Univ. Press, New York.

Wu, X., I. Simmonds, and W. Budd (1997), Modeling of Antarctic sea ice in a general circulation model, *J. Clim.*, *10*(4), 593–609.

Yen, Y.-C., (1981), Review of thermal properties of snow, ice and sea ice, *CRREL Rep. 81-10*, U.S. Army Cold Reg. Res. and Eng. Lab., Hanover, N. H.

Yen, Y.-C., K. C. Cheng, and S. Fukusako (1991), Review of intrinsic thermophysical properties of snow, ice, sea ice and frost, in *Proceedings of 3rd International Symposium on Cold Regions Heat Transfer*, edited by J. P. Zarling and S. L. Fausett, pp. 187–218, Univ. of Alaska Fairbanks, Fairbanks.

Zawilski, B., R. Littleton, and T. M. Tritt (2001), Description of the parallel thermal conductance technique for the measurement of the thermal conductivity of small diameter samples, *Rev. Sci. Instrum.*, *72*(3), 1771–1775.

T. G. Haskell, Industrial Research Limited, PO Box 31-310, Lower Hutt, New Zealand.

D. J. Pringle, Arctic Region Supercomputing Center and Geophysical Institute, University of Alaska Fairbanks, PO Box 756020, Fairbanks, AK 99775, USA. (pringle@gi.alaska.edu)

H. J. Trodahl, School of Chemical and Physical Sciences, Victoria University of Wellington, PO Box 600, Wellington, New Zealand.